ChemComm

Anionic Ligand-Induced Chirality in Perovskite Nanoplatelets

Journal:	*ChemComm*
Manuscript ID	CC-COM-10-2022-005469.R2
Article Type:	Communication

COMMUNICATION

Anionic Ligand-Induced Chirality in Perovskite Nanoplatelets

Thi Kim Tran Tran,[a] Joseph A. Adewuyi, [a] Yongchen Wang, [a] M. Daniela Morales-Acosta,[b] Tomoyasu Mani, [a] Gaël Ung, [a] Jing Zhao [a] *

Received 00th January 20xx,
Accepted 00th January 20xx

DOI: 10.1039/x0xx00000x

Perovskite materials passivated by chiral ligands have recently shown unique chiroptical activity with promising optoelectronic applications. However, the ligands have been limited to chiral amines. Here, chiral phosphate molecules have been exploited to synthesize $CsPbBr_3$ nanoplatelets. The nanoplates showed distinct circular dichroism signal and maintained their chiroptical properties after purification with anti-solvent.

Halide perovskites are known for their outstanding electronic and optical properties with promising applications in photovoltaics and optoelectronics such as solar cells,[1] light-emitting diodes (LEDs),[2] and photodetectors.[3] Their general chemical formula is ABX_3, where A is a monovalent cation such as methylammonium $CH_3NH_3^+$ (MA^+), formamidinium $HC(NH_2)_2^+$ (FA^+), or cesium (Cs^+), B is a divalent cation (e.g. Pb^{2+} or Sn^{2+}, etc.), and X is a halide anion (Cl^-, Br^-, or I^-). Among different perovskites, halide perovskite materials with chiral property are attractive for spintronic devices,[4] circularly polarized photodetectors[5] and circularly polarized light sources.[6] Chirality in halide perovskites is typically obtained by incorporating chiral organic molecules into perovskite structures to break their inversion symmetry. As a result, chirality is induced in the inorganic structures so that they exhibit chiroptical properties in the visible to near-IR region.[7,8]

Up to now, there are two approaches to induce chirality in perovskite materials. One is by introducing chiral organic cations into the A sites of perovskite framework. These cations isolate the single metal halide octahedra ($[BX_6]^{4-}$) layers which get stacked by van der Waals interactions between the chiral organic cations. For example, *R*/*S*-methylbenzylammonium (*R*/*S*-MBA) cations were placed in the A-sites to induce the chirality in two-dimensional (2D) lead- and tin-based perovskite thin films[9–12] and bulk single crystals[13]. Besides MBA, the other chiral ammonium cations used to build chiral perovskites were derived from (*R*/*S*)-(+)-sec-butylamine,[10] (*R*/*S*)-β-methylphenethylamine,[14,15] and (*R*/*S*)-1-(2-naphthyl)ethylamine.[11] However, these 2D perovskite films have shown low photoluminescence quantum yields due to significant nonradiative recombination resulting from surface and defect states.[16] The second approach was developed to overcome this problem, where the perovskite materials are passivated with chiral cation ligands. For example, *R*/*S*-MBA and (*R*/*S*)-1-(2-naphthyl)ethylamine were used as chiral ligands to enclose $MAPbBr_3$[4,17] and $MAPbI_3$[18] 2D perovskites, respectively. This approach was also applied in chiral three-dimensional perovskite nanocrystal (PNC) synthesis, such as (*R*/*S*)-1,2-diaminocyclohexane for $CsPb(I/Br)_3$ NCs,[19] (*R*/*S*)-α-octylamine for $CsPbBr_3$ NCs[20] and $FAPbBr_3$ NCs[21]. These all showed chiroptical properties and higher photoluminescence quantum yields. Although (*R*/*S*)-α-octylamine capped and $FAPbBr_3$ NCs[21] have shown the highest degree of circularly polarized emission, purification of the NCs with anti-solvent (ethyl acetate) removed a considerable amount of the chiral amine ligands and extinguish the chiraloptical properties.[21]

So far, all of the chiral molecules used to induce chirality in perovskite NCs are amines.[7,8] In order to understand and develop chiral perovskite materials for optical applications, it is necessary to expand the selection of chiral ligands. Some studies have shown that axially chiral binaphthyl derivatives could induce chirality in metal clusters, nanoparticles and nanorods.[22–25] Therefore, we adopted these anionic binaphthyl-based ligands for perovskite NC synthesis in this work. In particular, (*R*)-(−)-1,1′-binaphthyl-2,2′-diyl hydrogenphosphate (*R*-BNP) and *S*-BNP molecules (see the structures in Figure 1a) were prepared following a published protocol[26] and characterized by nuclear magnetic resonance (NMR) (see details in the SI). They were then used to synthesize $CsPbBr_3$ nanoplatelets (NPLs). The NPLs with the *R*- and *S*-BNP ligands exhibit circular dichroism (CD) signal of opposite signs at 350 - 460 nm wavelength beyond the absorption range of BNPs, demonstrating their chiral properties. Moreover, the chirality of the NPLs was maintained after purification with anti-solvent because the phosphate groups are known to have high binding affinity to $CsPbBr_3$ perovskite

[a] *Department of Chemistry, University of Connecticut, 55 North Eagleville Rd., Storrs Mansfield, Connecticut 06269-3060, USA. Email: jing.zhao@uconn.edu*
[b] *Institute of Materials Science, University of Connecticut, Storrs Mansfield, Connecticut 06269, USA.*

†Electronic Supplementary Information (ESI) available: Experimental details and additional NMR, TEM, FTIR and fluorescence anisotropy analysis. See DOI: 10.1039/x0xx00000x

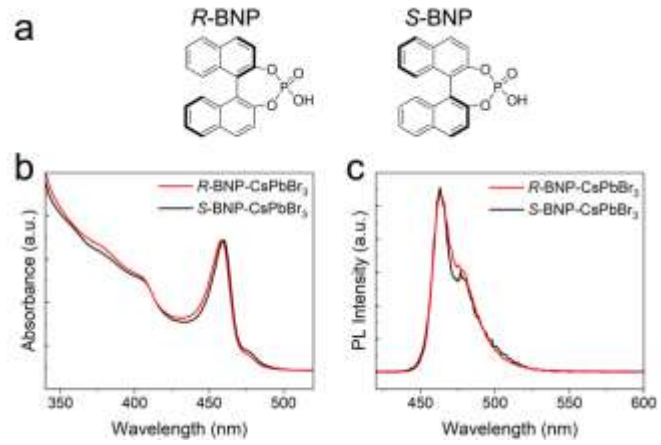

Figure 1. (a) Chemical structures of BNP ligand with (*R*) and (*S*) enantiomers. (b) Absorption and (c) photoluminescence (PL) spectra of *R*- (red curves) and *S*- (black curves) BNP- $CsPbBr_3$ NPLs in hexane.

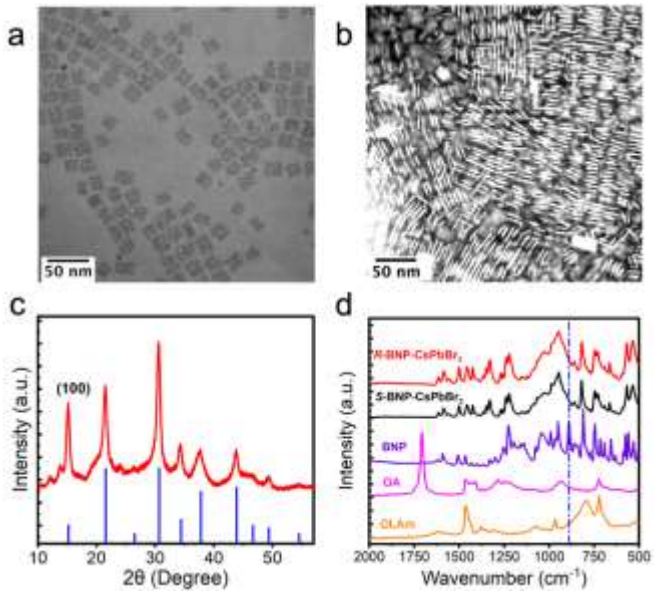

Figure 2. (a) TEM image of BNP-$CsPbBr_3$ NPLs lying on their "flat" side. (b) STEM dark-field image of BNP-$CsPbBr_3$ NPLs in stacks. (c) XRD spectrum of BNP-$CsPbBr_3$ NPLs. The reference cubic crystal structure of $CsPbBr_3$ is shown in blue lines, PDF 00-054-0752. (d) FTIR spectra of OLAm, OA, BNP and BNP-$CsPbBr_3$ NPLs.

NC surface in various binding modes.[27–31] Furthermore, the NPLs show linearly polarized emission in their PL, which is ascribed to their anisotropic shape. This work provides alternative means to develop chiral perovskite materials.

The NPLs were synthesized using a hot injection method modified from the protocol reported by Protesescu *et al.*[32] Firstly, Cs-OA-*R/S*-BNP precursor in 1-octadecene (ODE) was prepared by dissolving Cs_2CO_3, oleic acid (OA) and *R/S*-BNP in ODE at 110 °C. In a separate three-neck flask attached to a Schlenk line, $PbBr_2$ was mixed with 1:1 molar ratio of oleylamine (OLAm) and *R/S*-BNP and dissolved in solvent ODE. After degassing at 110 °C for 1h, the mixture was heated to 175 °C under N_2 for 30 mins in order to ensure complete dissolution. The temperature of the mixture was brought down to 120 °C, and the Cs-OA-*R/S*-BNP precursor was swiftly injected. After 7 s, the reaction mixture was quenched by a water-ice bath. The NPLs were purified from the reaction mixture through precipitation with tert-butanol as the anti-solvent and centrifugation. The precipitate was redispersed in hexane for characterization.

The UV-vis absorption and PL spectra of *R*- and *S*-BNP-$CsPbBr_3$ NPLs in hexane are shown in Figure 1 b and c. The corresponding spectra look almost identical for the *R*- and *S*-BNP NPL samples, suggesting that the morphology of the two samples are similar. The absorption spectra peak at 460 nm and the PL peak at 464 nm, which corresponds to 5 unit-cell thickness of $CsPbBr_3$ NPLs as shown in previous report.[33] The sharp excitonic absorption is for a result of quantum confinement effect in the NPLs with the thickness much less than the bulk $CsPbBr_3$ Bohr exciton diameter (7 nm[32]). The shoulder in the absorption and PL spectra at 475 and 479 nm, respectively, coincide with each other that is presumably caused by accumulation and transformation of some of the thin NPLs to thicker ones during the purification step. Similar phenomenon was observed by Wang *et al.*[34] Thus, the final product primarily consists of 5 unit-cell thick NPLs, with a small portion of aggregates. The PL quantum yield is 43 % and 34% with respect to *R*- and *S*- BNP NPLs. The PL lifetime of *R*- and *S*- BNP NPLs were 5.89 ns and 6.14 ns respectively, determined by fitting a bi-exponential function of the PL decays. The fitting parameters are listed in Table S1.

The morphology of the NPLs was studied with transmission electron microscopy (TEM). The TEM images were acquired from a diluted sample where the NPLs lied flat on the TEM grid (2a) and from a concentrated sample where the NPLs stacked (2b). The TEM images revealed the platelet morphology of BNP-$CsPbBr_3$ NCs, with a lateral dimension of 10-20 nm and an average thickness of 2.7±0.4 nm (see thickness distribution in Figure S6). The X-ray diffraction (XRD) peaks of BNP-$CsPbBr_3$ NPLs in Figure 2c match well with that of cubic $CsPbBr_3$. In the cubic phase, the lattice constant of $CsPbBr_3$ NPL unit cells, which is equal to lattice spacing between the {100} planes, is calculated to be 0.585 nm. Therefore, the thickness of BNP-$CsPbBr_3$ NPLs (~2.7 nm) corresponds to approximately 5 unit cells, which is in an agreement with the previous report[33] and the features in the UV-vis absorption spectra in Figure 1b.

To study the surface chemistry of BNP-$CsPbBr_3$ NPLs, FTIR spectroscopy was performed and the spectra are shown in Figure 2d and S6. The spectra of the BNP-NPLs show much similarity to that of the BNP molecules, proving that BNP molecules have been successfully incorporated in the NPLs. Specifically, the stretching vibration of P-O-H at 889 cm^{-1} disappeared in BNP-NPLs in contrast to BNP ligand, suggesting the deprotonation of hydrogen phosphate group of BNP by OLAm.[35] Meanwhile, the stretching vibration mode of P=O (~1000 cm^{-1}) and P-O (~ 750 cm^{-1}), and the bending vibration mode of O-P-O (~ 550 cm^{-1}) in BNP-NPLs are present but broader than those of the BNP molecules, likely because of the different local chemical environments around the BNP molecules after they were attached to the NPL surface.[35] Moreover, even though OA was used in cesium precursor preparation, the stretching vibration of C=O at 1706 cm^{-1} was not observed probably due to lower affinity to the NPL surface of carboxyl groups compared to

phosphor-based ones.[31] The broad peak at 3159 cm^{-1} (Figure S7) was attributed to N^{+}-H_3 stretching vibrations of ammonium groups of protonated OLAm on the NPLs.[36] Therefore, BNP and

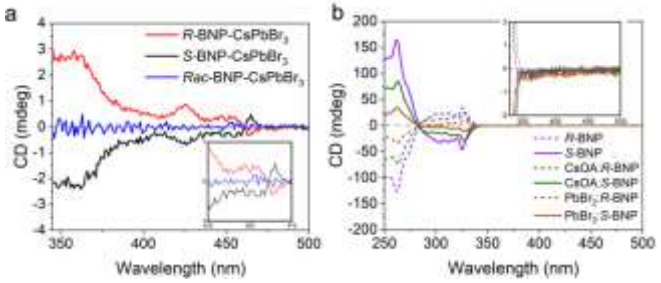

Figure 3. CD spectra of (a) *R*- and *S*-BNP-$CsPbBr_3$ NPLs (inset 425 – 475 nm) and (b) precursors (inset 330 – 500 nm).

OLAm ligands are present on the NPL surface.

Chirality of NPLs was evaluated by circular dichroism (CD) spectroscopy, in which the difference in absorbance of left- and right-handed circularly polarized light of a sample was recorded. CD spectroscopy is used to study chiroptical properties of materials in their ground state.[37] CD spectra of BNP-$CsPbBr_3$ NPLs and precursors are shown in Figure 3. The *R*-BNP and *S*-BNP capped NPLs exhibit CD spectra above 350 nm that are mirror images with almost equal intensity. In contrast, the CD signal of free *R/S*-BNP molecules and precursors in the synthesis only has peaks below 340 nm. Cotton effect, which is a characteristic change of CD sign in the vicinity of an absorption band of a substance, is observed at 461 nm which is around the first excitonic absorption of the NPLs. Moreover, NPLs were also prepared with racemic mixture of the *R/S*-BNP ligands, and they showed no CD features. Therefore, we confirmed that chirality of the NPLs has been induced by of *R/S*-BNP ligands.

In previous studies of chiral $CsPbBr_3$ perovskite NCs, it was proposed that chiral ammonium ligands occupy the A-site of the perovskite structure and transfer chirality via two mechanisms. One is asymmetric lattice distortions up to five atomic unit cells deep into the PNCs by chiral ammonium ligands.[38] The other one is the electronic state hybridization between the valence band of perovskite NCs and the HOMO of chiral ligands.[39] In this study, the BNP molecules have two bulky naphthyl groups and a bridged structure of two oxygen atoms connected at the 2,2'-positions of the binaphthyl rings via a -P(O)(OH) moiety. Considering steric hindrance, it is likely that BNP molecules only bind to uncoordinated Pb^{2+} and Cs^{+} on the NPL surface and do not get into halide vacancies on the surface. Still, BNP molecules on the NPL surface can induce chirality in $CsPbBr_3$ perovskite NCs via both mechanisms mentioned above. Future mechanistic studies are necessary to elucidate the interaction between anionic BNP and the $CsPbBr_3$ NCs.

In addition to chirality in the ground state absorption of the NPLs, we observed fluorescence anisotropy in the excited state of NPLs as shown in Figure 4. Fluorescence anisotropy has been observed in some anisotropic semiconductor nanocrystals such as $CsPbBr_3$ and CdSe/CdS core/shell nanorods[40,41] ; however, this property has yet to be explored in halide perovskite NPLs.

In our experiment, linearly polarized emission of the NPLs was characterized by exciting them with linearly polarized light and comparing the photoluminescence intensity through parallel and

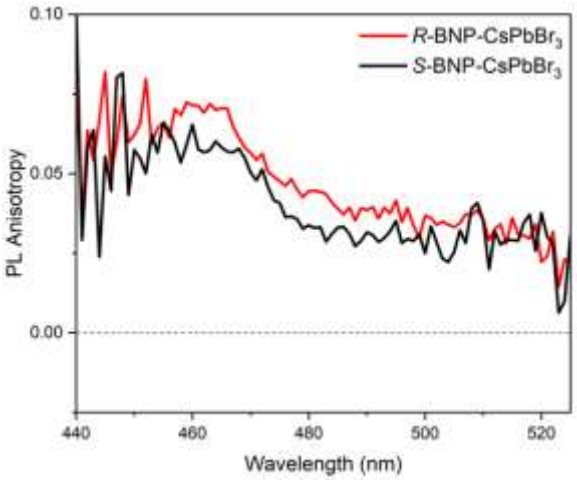

Figure 4. Photoluminescence anisotropy of $CsPbBr_3$ NPLs.

perpendicular polarizers (see details in the Experimental Section in the SI). The NPLs of 5 monolayer thick achieve a fluorescence anisotropy value of ~ 0.06. In contrast, fluorescence anisotropy was not observed in cubic shaped $CsPbBr_3$ NCs (see Figure S8). Thus, the fluorescence anisotropy is attributed to the in-plane orientation of the transition dipole moments[42] and the small height of the NPLs compared to their base. Both chirality in the ground state and linearly polarized emission from the excited state of the *R/S*-BNP-$CsPbBr_3$ NPLs open more possibilities for using them in display applications.

In conclusion, we developed a new approach to fabricate chiral perovskite NCs by using anionic ligands with high affinity to perovskite surface. The *R/S*-BNP ligands successfully induced chiroptical activity in five-unit cell $CsPbBr_3$ NPLs. The BNP-$CsPbBr_3$ NPLs showed CD signals after purification with t-butanol as the anti-solvent. Linearly polarized emission of the NPLs was also observed and ascribed to their anisotropic shape. This study has expanded the choice of chiral ligands for perovskite NCs from cationic amine to anionic phosphate. It opens up the possibility to achieve chiroptical perovskite NCs using chiral phosphorus-based ligands with high affinity to the perovskite surface.

JZ and GU acknowledge partial financial support from the National Science Foundation (CHE-1554800 and CHE- 2203854 for JZ, CHE-2041084 for GU) for this work. We thank Miss Hawi Nyiera for her assistance with the PL decay measurements.

Author Contributions

TKT.T. and J.Z. initiated the project. TKT.T. conducted NPL synthesis, characterization and analyzed the results under the supervision of J.Z. J.A. synthesized BNP molecules and performed NMR characterization of BNP under the supervision of G.U. Y.W. and TKT.T. collected TEM images. D.M. and TKT.T. carried out XRD measurement. T.M. performed linearly

polarized emission measurement. All authors contributed to the manuscript preparation. All authors gave approval to the final version of the manuscript.

Conflicts of interest

There are no conflicts to declare.

Notes and references

1 J. Y. Kim, J.-W. Lee, H. S. Jung, H. Shin and N.-G. Park, *Chem Rev*, 2020, **120**, 7867–7918.
2 G. Pacchioni, *Nat Rev Mater*, 2021, **6**, 108.
3 J. Miao and F. Zhang, *J Mater Chem C Mater*, 2019, **7**, 1741–1791.
4 G. Long, C. Jiang, R. Sabatini, Z. Yang, M. Wei, L. N. Quan, Q. Liang, A. Rasmita, M. Askerka, G. Walters, X. Gong, J. Xing, X. Wen, R. Quintero-Bermudez, H. Yuan, G. Xing, X. R. Wang, D. Song, O. Voznyy, M. Zhang, S. Hoogland, W. Gao, Q. Xiong and E. H. Sargent, *Nat Photonics*, 2018, **12**, 528–533.
5 C. Chen, L. Gao, W. Gao, C. Ge, X. Du, Z. Li, Y. Yang, G. Niu and J. Tang, *Nat Commun*, 2019, **10**, 1927.
6 I. C. Seo, Y. Lim, S.-C. An, B. H. Woo, S. Kim, J. G. Son, S. Yoo, Q.-H. Park, J. Y. Kim and Y. C. Jun, *ACS Nano*, 2021, **15**, 13781–13793.
7 Y. Dong, Y. Zhang, X. Li, Y. Feng, H. Zhang and J. Xu, *Small*, 2019, **15**, 1902237.
8 G. Long, R. Sabatini, M. I. Saidaminov, G. Lakhwani, A. Rasmita, X. Liu, E. H. Sargent and W. Gao, *Nat Rev Mater*, 2020, **5**, 423–439.
9 J. Ma, C. Fang, C. Chen, L. Jin, J. Wang, S. Wang, J. Tang and D. Li, *ACS Nano*, 2019, **13**, 3659–3665.
10 J. Ahn, E. Lee, J. Tan, W. Yang, B. Kim and J. Moon, *Mater Horiz*, 2017, **4**, 851–856.
11 J. Ahn, S. Ma, J.-Y. Kim, J. Kyhm, W. Yang, J. A. Lim, N. A. Kotov and J. Moon, *J Am Chem Soc*, 2020, **142**, 4206–4212.
12 H. Lu, C. Xiao, R. Song, T. Li, A. E. Maughan, A. Levin, R. Brunecky, J. J. Berry, D. B. Mitzi, V. Blum and M. C. Beard, *J Am Chem Soc*, 2020, **142**, 13030–13040.
13 Y. Dang, X. Liu, Y. Sun, J. Song, W. Hu and X. Tao, *J Phys Chem Lett*, 2020, **11**, 1689–1696.
14 H. Ren, Y. Wu, C. Wang and Y. Yan, *J Phys Chem Lett*, 2021, **12**, 2676–2681.
15 C. Yuan, X. Li, S. Semin, Y. Feng, T. Rasing and J. Xu, *Nano Lett*, 2018, **18**, 5411–5417.
16 G. Xing, B. Wu, X. Wu, M. Li, B. Du, Q. Wei, J. Guo, E. K. L. Yeow, T. C. Sum and W. Huang, *Nat Commun*, 2017, **8**, 14558.
17 Z. N. Georgieva, B. P. Bloom, S. Ghosh and D. H. Waldeck, *Advanced Materials*, 2018, **30**, 1800097.
18 T. Liu, W. Shi, W. Tang, Z. Liu, B. C. Schroeder, O. Fenwick and M. J. Fuchter, *ACS Nano*, 2022, **16**, 2682–2689.
19 T. He, J. Li, X. Li, C. Ren, Y. Luo, F. Zhao, R. Chen, X. Lin and J. Zhang, *Appl Phys Lett*, 2017, **111**, 151102.
20 W. Chen, S. Zhang, M. Zhou, T. Zhao, X. Qin, X. Liu, M. Liu and P. Duan, *J Phys Chem Lett*, 2019, **10**, 3290–3295.
21 Y.-H. Kim, Y. Zhai, E. A. Gaulding, S. N. Habisreutinger, T. Moot, B. A. Rosales, H. Lu, A. Hazarika, R. Brunecky, L. M. Wheeler, J. J. Berry, M. C. Beard and J. M. Luther, *ACS Nano*, 2020, **14**, 8816–8825.
22 A. Nemati, S. Shadpour, L. Querciagrossa, T. Mori, C. Zannoni and T. Hegmann, *ACS Nano*, 2019, **13**, 10312–10326.
23 C. Gautier, R. Taras, S. Gladiali and T. Bürgi, *Chirality*, 2008, **20**, 486–493.
24 T. Mori, A. Sharma and T. Hegmann, *ACS Nano*, 2016, **10**, 1552–1564.
25 M. Tamura and H. Fujihara, *J Am Chem Soc*, 2003, **125**, 15742–15743.
26 J. Jacques and C. Fouquey. Enantiomeric (S)-(+)- and (R)-(¬-)-1,1'-Binaphthyl-2,2'-diyl hydrogen phosphate. *Organic Syntheses*, Coll. Vol. 8, p.50 (1993); Vol 67, p.1 (1989).
27 F. Liu, Y. Zhang, C. Ding, S. Kobayashi, T. Izuishi, N. Nakazawa, T. Toyoda, T. Ohta, S. Hayase, T. Minemoto, K. Yoshino, S. Dai and Q. Shen, *ACS Nano*, 2017, **11**, 10373–10383.
28 B. Zhang, L. Goldoni, J. Zito, Z. Dang, G. Almeida, F. Zaccaria, J. de Wit, I. Infante, L. de Trizio and L. Manna, *Chemistry of Materials*, 2019, **31**, 9140–9147.
29 L. Wu, Q. Zhong, D. Yang, M. Chen, H. Hu, Q. Pan, H. Liu, M. Cao, Y. Xu, B. Sun and Q. Zhang, *Langmuir*, 2017, **33**, 12689–12696.
30 J. Y. Woo, S. Lee, S. Lee, W. D. Kim, K. Lee, K. Kim, H. J. An, D. C. Lee and S. Jeong, *J Am Chem Soc*, 2016, **138**, 876–883.
31 J. Shamsi, D. Kubicki, M. Anaya, Y. Liu, K. Ji, K. Frohna, C. P. Grey, R. H. Friend and S. D. Stranks, *ACS Energy Lett*, 2020, **5**, 1900–1907.
32 L. Protesescu, S. Yakunin, M. I. Bodnarchuk, F. Krieg, R. Caputo, C. H. Hendon, R. X. Yang, A. Walsh and M. v Kovalenko, *Nano Lett*, 2015, **15**, 3692–3696.
33 Q. A. Akkerman, S. G. Motti, A. R. Srimath Kandada, E. Mosconi, V. D'Innocenzo, G. Bertoni, S. Marras, B. A. Kamino, L. Miranda, F. de Angelis, A. Petrozza, M. Prato and L. Manna, *J Am Chem Soc*, 2016, **138**, 1010–1016.
34 Y. Wang, X. Li, S. Sreejith, F. Cao, Z. Wang, M. C. Stuparu, H. Zeng and H. Sun, *Advanced Materials*, 2016, **28**, 10637–10643.
35 M. Klähn, G. Mathias, C. Kötting, M. Nonella, J. Schlitter, K. Gerwert and P. Tavan, *J Phys Chem A*, 2004, **108**, 6186–6194.
36 L. M. Wheeler, E. M. Sanehira, A. R. Marshall, P. Schulz, M. Suri, N. C. Anderson, J. A. Christians, D. Nordlund, D. Sokaras, T. Kroll, S. P. Harvey, J. J. Berry, L. Y. Lin and J. M. Luther, *J Am Chem Soc*, 2018, **140**, 10504–10513.
37 Y. Sang, J. Han, T. Zhao, P. Duan and M. Liu, *Advanced Materials*, 2020, **32**, 1900110.
38 Y.-H. Kim, R. Song, J. Hao, Y. Zhai, L. Yan, T. Moot, A. F. Palmstrom, R. Brunecky, W. You, J. J. Berry, J. L. Blackburn, M. C. Beard, V. Blum and J. M. Luther, *Adv Funct Mater*, 2022, **32**, 2200454.
39 S. Jiang, Y. Song, H. Kang, B. Li, K. Yang, G. Xing, Y. Yu, S. Li, P. Zhao and T. Zhang, *ACS Appl Mater Interfaces*, 2022, **14**, 3385–3394.
40 Y. Dou, F. Cao, T. Dudka, Y. Li, S. Wang, C. Zhang, Y. Gao, X. Yang and A. L. Rogach, *ACS Mater Lett*, 2020, **2**, 814–820.
41 P. D. Cunningham, J. B. Jr. Souza, I. Fedin, C. She, B. Lee and D. v Talapin, *ACS Nano*, 2016, **10**, 5769–5781.
42 A. H. Proppe, G. W. Walters, A. Y. Alsalloum, A. A. Zhumekenov, E. Mosconi, S. O. Kelley, F. de Angelis, L. Adamska, P. Umari, O. M. Bakr and E. H. Sargent, *J Phys Chem Lett*, 2020, **11**, 716–723.

